J Mater Sci (2008) 43:1460–1470
DOI 10.1007/s10853-007-2307-1

ZnO low-dimensional structures: electrical properties measured inside a transmission electron microscope

Pedro M. F. J. Costa · Dmitri Golberg · Guozhen Shen · Masanori Mitome · Yoshio Bando

Received: 16 May 2007 / Accepted: 9 November 2007 / Published online: 12 December 2007
© Springer Science+Business Media, LLC 2007

Abstract The electrical properties of wurtzite-type ZnO low-dimensional structures were analysed using a scanning tunnelling microscopy (STM) in situ holder for transmission electron microscopes (TEM). Compared to similar studies in the literature employing nanowires or nanobelts, our work illustrates that rather complex structures can be reliably analysed with this technique. Through controlled contact manipulations it was possible to alter the systems *I–V* characteristics and, in separate experiments, to follow their electrical response to cycles of induced stress. Analysis of the *I–V* curves showed higher than expected resistances which, according to the detailed TEM characterisation, could be correlated with the considerable density of defects present. These defects accumulate in specific areas of the complex structural arrays of ZnO and represent high resistance points responsible for structural failure, when the systems are subjected to extreme current flows.

Introduction

Wurtzite ZnO is a semiconductor of the II–VI family characterized by a direct bandgap of 3.37 eV at room temperature and a large exciton binding energy of 60 meV. These properties, together with a thermal energy at room temperature (RT) of 26 meV, should ensure a highly efficient RT excitonic emission. Consequently, ZnO has been actively investigated for applications in optoelectronics [1, 2]. Currently, the generality of commercial semiconductor-based optoelectronic products such as light-emitting diodes and lasers rely on complex processing of hetero-epitaxially grown layered structures. This growth method inherently results in accumulated strain due to lattice mismatches. Unfortunately, one of the most common strain relief mechanisms is the generation of dislocations. These are highly undesirable for optoelectronic applications as they can act as non-radiative recombination centres [1]. In contrast to layered materials, a significant number of ZnO one-dimensional nanostructures have been reported where dislocations are absent [3] and which have, furthermore, shown promising optical properties [4]. An additional property of wurtzite ZnO is the presence of an electric field along the c-axis due to its non-centrosymmetric structure. There is, along the alternated layers of Zn and O, a normal dipole moment, which is responsible for the spontaneous polarisation effect and subsequently accounts for the presence of the ZnO (0001) polar surfaces. The presence of this spontaneous electric field along [0001] could lead to measurable orientation-dependent variations in the current transport for quasi-one-dimensional ZnO materials.

Piezo-holders are exciting tools that enable mechanical and electrical properties measurements inside a TEM [5]. As such, it is possible to perform scanning probe microscopy or indentation analyses on very small volumes whilst continuously imaging the object of study [6, 7]. In recent reports, astonishing properties of nanostructures were described such as the superplasticity of carbon nanotubes [8]. Relevant studies, which explored the electrical properties of ZnO nanowires, also have been carried out [9]. Nonetheless, most researchers have focussed on simple

Electronic supplementary material The online version of this article (doi:10.1007/s10853-007-2307-1) contains supplementary material, which is available to authorized users.

P. M. F. J. Costa (✉) · D. Golberg · G. Shen · M. Mitome · Y. Bando
Nanoscale Materials Center, National Institute for Materials Science, 1-1 Namiki, Tsukuba, Ibaraki 305-0044, Japan
e-mail: costa.pedro@nims.go.jp

structures such as ZnO nanobelts and nanowires [9–11]. Moreover, the number of orientations probed has been rather limited, i.e. mainly along [0001], and little mention has been made to the possible influence of structural defects. These two factors could potentially have a significant effect on the electrical properties measured for ZnO nanostructures.

In the present report, the structural characterisation of complex wurtzite-type ZnO structures with low-dimensional geometries is described followed by the in situ analysis of their *I–V* characteristics using a STM/TEM holder. Different crystal orientations were probed which, added to the considerations made for the presence of defects, electron beam effects and current-induced structural failure, show that the measured electrical properties of these structures are dominated by defect density and, furthermore, highly dependent on contact characteristics.

Experimental

Two samples were selected in view of their structural complexities and both included arrays of nanostructured ZnO low-dimensional objects. For sample A, the structures were grown using a metal vapour deposition (MVD) process. Metallic zinc powder (100 mesh, 99.998%, Aldrich) was placed in a quartz crucible inside a horizontal tubular furnace. This was then sublimed at 550 °C redepositing downstream in a Si substrate as white-powder ZnO. The reactive gas/carrier was an O_2/Ar flow (additional details on growth and characterisation can be found in [12]). Sample B was grown as part of a separate set of synthesis experiments. Details are as described in [13] with the exception that an O_2/Ar flow (O_2: 30 sccm, Ar: 350 sccm) was used instead of pure Ar.

Conversely to previous work carried out on boron nitride nanotubes by us [14], the structural characterisation of the ZnO materials was performed separately from the electrical measurements. This was necessary since it was not always possible to find structures oriented close to an appropriate high symmetry zone-axis. In contrast to nanotubes, which ideal structure is radially symmetric, a precise orientation of the lattice planes parallel to the electron beam for inorganic crystals such as ZnO is crucial. Since the STM/TEM holder is of single-tilt type this strongly limits TEM structural analysis for anisotropic inorganic crystals such as ZnO. The structural data was acquired during operation, at 300 kV, of a JEOL JEM-3000F, with a point resolution of 2.0 Å. In order to avoid solvent contaminations, the sample was prepared using a dry-contact method and a Lacey Carbon Cu grid. As regards the spectroscopical studies these were performed in a JEOL JEM-3100FEF, operated at 300 kV and with a point resolution of 1.7 Å. This microscope is equipped with an Omega Filter and a 1k slow-scan charge coupled device (CCD) camera [15]. The side-entry piezoholder used has STM capabilities and is commercialised by Nanofactory Instruments AB [16]. In our set-up, a sharp Au wire (250 µm diameter) acts as the stationary tip-electrode which has biasing capabilities (Fig. 1). The ZnO sample was mounted on the opposite electrode, this consisting of a grounded Au wire (same diameter as the tip) fixed on a movable part with six springs [14]. In order to improve the electrical contact and avoid contaminations, the end of the Au wire was cut flat and covered with an electrically conductive paste immediately before loading the sample. A gentle touch of the Au wire flat end on the Si substrate surface (which contained the ZnO structures) enabled an efficient sample transfer. The choice of Au electrodes, which served as contacts for the *I–V* measurements, is justified by the Schottky-Mott model which predicts that metals with high work functions are key candidates for rectifying contacts on *n*-type semiconductors. Concerning ZnO, these metals should additionally possess a low oxygen affinity since the *n*-type conductivity of this oxide has traditionally been attributed to native defects such as oxygen vacancies and zinc interstitials [17]. Hence the materials of choice are usually limited to gold, platinum and palladium [18]. From these, Au is possibly the most convenient to use. For our preparations, we avoided the use of organic solvents. Although better dispersions are expected, their use may lead to surface contamination which can potentially change the materials' electrical properties. It should be noted that, in the preparation of these samples, it is desirable that a low density of representative and individually dispersed structures is loaded onto the Au wire flat surface. This unfortunately is not always achievable, in particular, if the substrates contain a

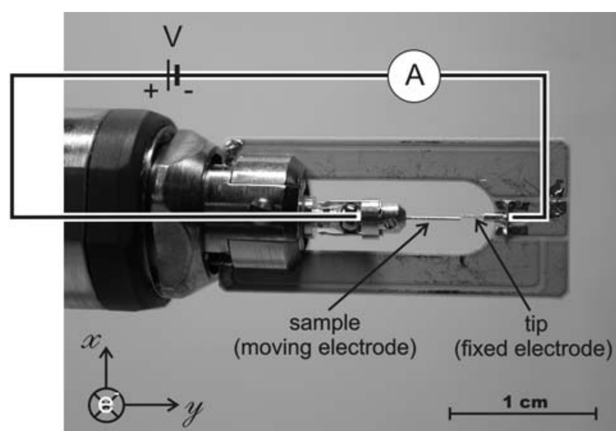

Fig. 1 Diagram of the single tilt STM/TEM holder. Both electrodes are cut from 250 µm thick Au wires. The direction of the imaging electron beam is normal to the x,y plane of the holder

very high density of structures or these are highly bundled together.

In addition to the *I–V* measurements, experiments to analyse the electron current density during specimen imaging were also carried out. This was done using a retractable Faraday cup mounted on the viewing chamber of the JEOL JEM-3100FEF. Besides the Faraday cage, the current density was also controlled with the help of a previously calibrated focus screen.

Results

Structural analysis

Sample A

Several ZnO arrays and nail-shaped isolated structures were analysed (Fig. 2a). The arrays are characterised by a primary and extended basal ZnO square column, which acts as a template layer for the growth of secondary nail-shaped structures (a cross-sectional diagram is shown in Fig. 2a; cf. with Fig. 2f). Only one side of this basal template-column is growth active. Although numerous nail-shaped structures were seen to be fused together, ZnO is a brittle material and fractures are therefore expected, explaining the widespread presence of isolated structures. It was observed that the nails consistently showed closed hexagonal packed structure with a general growth direction of ⟨0001⟩ (Fig. 2b–e). In addition to this, and after detailed interpretation of several convergent beam electron diffraction (CBED) patterns taken at the ⟨01−10⟩ zone-axis, it was concluded that the top of the hexagonal heads are (0001)-Zn surfaces. From Fig. 2h–j, it is seen that the experimental 0002 and 000-2 disks, which differ in intensity distribution due to the wurtzite non-centrosymmetrical structure, are commensurate with the Bloch-wave theoretically calculated patterns. (0001)-Zn surfaces of ZnO have already been reported recently as being chemically active and can furthermore account for the self-catalytic growth of nanostructures [19]. It is interesting to notice from the plan-view images of the arrays that the hexagonal heads of the nails would invariably be fused through their vertices, which correspond to the ⟨−2110⟩ direction (Fig. 2a). This would further imply that the major axis of the ZnO basal template column should also correspond to ⟨−2110⟩. Notwithstanding, in several cross-sectional views, besides the predominant ⟨−2110⟩ growth direction for the basal column, it was also possible to identify some structures where the major axis of growth was ⟨10−10⟩. In brief, and as concerns the arrays of sample A, the microscopical analysis shows that whilst the basal template column grows either on the ⟨−2110⟩ or ⟨01−10⟩ directions, the nail-shaped structures are invariably grown on [0001] and terminated in hexagonal heads with (0001) zinc surface planes.

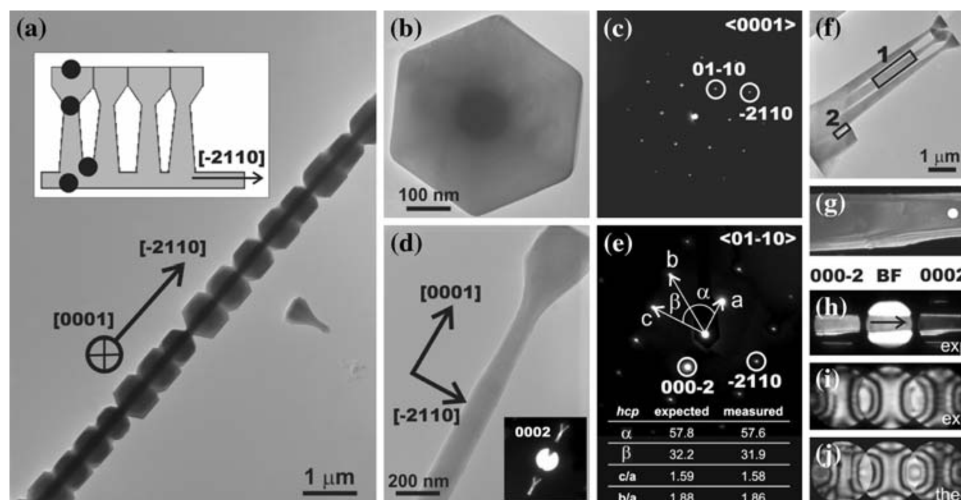

hcp	expected	measured
α	57.8	57.6
β	32.2	31.9
c/a	1.59	1.58
b/a	1.88	1.86

Fig. 2 (**a**) Plan-view image of a sample A array. Besides the hexagonal heads it is also possible to observe the line contrast due to the primary basal template column from which the nail-shaped structures grow. Inset: cross-section schematics of the array; the black dots represent areas analysed by EDX. (**b**) Plan-view of an individual hexagonal head. (**c**) Diffraction pattern (DP) of (**b**) showing that the facets are {01−10}-type planes. (**d**) Cross-sectional view of an isolated nail-structure. Inset: defocused DP confirming the [0001] growth direction. (**e**) DP of (**d**). The table confirms the zone-axis and reflections assignment. (**f**) Cross-section of a partial array. (**g**) Weak beam dark field image, with $g(2g) = 000{-}2$, taken from area 1 in (**f**) and illustrating the absence of dislocations. The white dot shows the area probed by CBED. The thickness of the structure at this point is 238 nm, as interpreted through CBED. (**h**) Defocused DP taken from the area boxed in (**f**). The central disk corresponds to the bight field image (transmitted beam) whereas the 000−2 disk is equivalent to image (**g**). (**i**) Experimental CBED taken on zone axis ⟨01−10⟩. (**j**) Simulated CBED pattern for the experimental image in (**i**). Parameters for the WebEmaps software used were: Bloch-coherent calculation, disk radius = 1.3, tilt = (0,0,0.8), sampling = 24

In order to identify whether plastic deformation was present in both arrays and isolated nails, we carried out extensive dark field analysis. In this process, two reciprocal (g) vectors were used, g = −2110 and g = 0002, both readily available from the ⟨01−10⟩ zone-axis. It is known that, for wurtzite-type structures, the study of these reciprocal lattice vectors will provide sufficient information to determine both the presence and nature of the dislocations in the material [1]. Weak beam dark field (WBDF) analysis showed that the nails are clear from dislocations (a partial view of a representative WBDF image taken at g(2g) = 000−2 is shown in Fig. 2g). In the case of the arrays, dislocations are present in the junction of the nails with the primary basal column, most commonly when the base of two nails would meet (Fig. 3). This may be an effect of small misorientations between the facets of neighbouring nails. The accumulated strain during growth is relieved through the generation of dislocations. These dislocations are mainly of mixed (edge plus screw components present) and pure-edge nature i.e. visible only under g = −2110 (cf. Fig. 3a vs. 3b).

As regards the chemical composition of this sample, several areas were probed using energy dispersive X-ray spectroscopy (EDX) (spectra not shown). Despite the use of the 4d transition metal indium in the original synthesis of the ZnO structures [12], this element could not be detected. It is known that the minimum mass fraction (or detection limit) for this spectroscopical technique is around 1 wt.% (when used in routine operation) [20]. This means that it is not possible to exclude having substitutional sites of indium in the ZnO structure or even the formation of very small In clusters dispersed throughout the crystal surfaces. A growth mechanism based on this assumption was proposed by Shen et al. [12] which, furthermore, attempts to explain the formation of the nail-shaped structures.

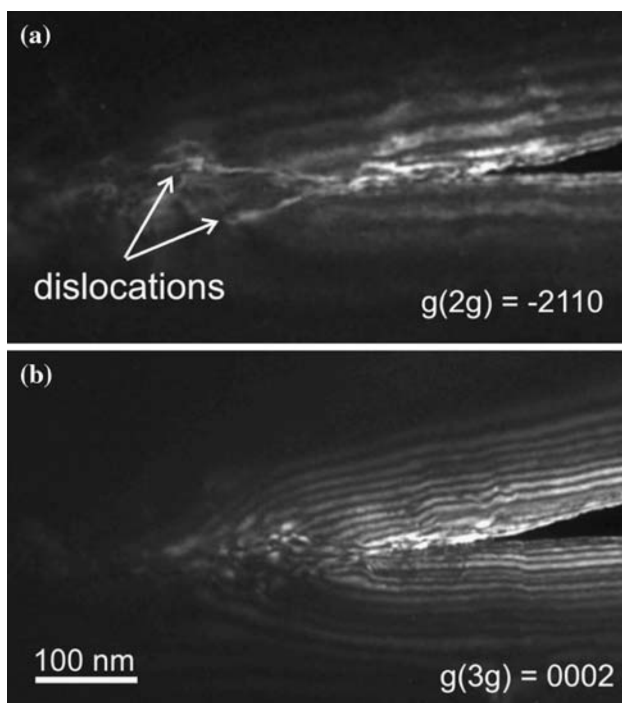

Fig. 3 (**a**) WBDF image taken with $g(2g) = -2110$ conditions from region 2 in Fig. 2f; (**b**) Same area as in (**a**) but with $g(3g) = 0002$. The dislocations are now invisible because $g.b = 0$, where b represents the Burgers vector of the dislocations

In a final note for sample A, no thick amorphous layers were seen to cover the nails nor the arrays. The presence of these could have a significant effect in the measured electrical characteristics.

Sample B

Similar to the products of sample A, this sample presented numerous arrays of nanowires from where secondary structures would grow. Again, the secondary growth was invariably occurring on one side, this time restricted to particular active areas of the basal nanowires (Fig. 4a). The morphology of the branches varied from straight wires to baseball-bat shaped structures, others resembling nails (Fig. 4b–d). Notwithstanding, they showed unique growth direction [0001], commensurate with the nails observed in sample A. Numerous secondary structures were found isolated with some showing facets with asymmetric surface roughness (Fig. 4e). This is not believed to be due to surface reconstruction, as reported for other ZnO structures [3], but rather a consequence of the abrupt detachment of the branches from the array.

Interestingly, and conversely to most known ZnO nanostructures, which usually grow along one of the high-symmetry ⟨0−110⟩, ⟨0001⟩ or ⟨−2110⟩ axis, the basal nanowires were seen to have inconsistent growth direction (cf. defocused diffraction pattern in Fig. 4a, inset). The growth axis would often change throughout the length of the nanowires particularly whenever kinks or other major structural defects were present. Nonetheless, and as it can be observed from Fig. 4b, it was found that the secondary structures would generally grow with their axis at ca. 40° from the basal nanowires and joined at the base through a few unit cells thick ZnO layers. This area, containing the interface between primary and secondary structures, was populated by dislocations and other types of defects such as thick surface steps. The inset in Fig. 4b shows a representative area where Moiré fringes are present. These interference fringes are usually either a result of the overlap of lattices with different parameters and/or when domains with the same structure are rotated by a few degrees. In our case, the interference pattern may be accounted for by the rotation of the ZnO g-vectors. Furthermore, the presence of

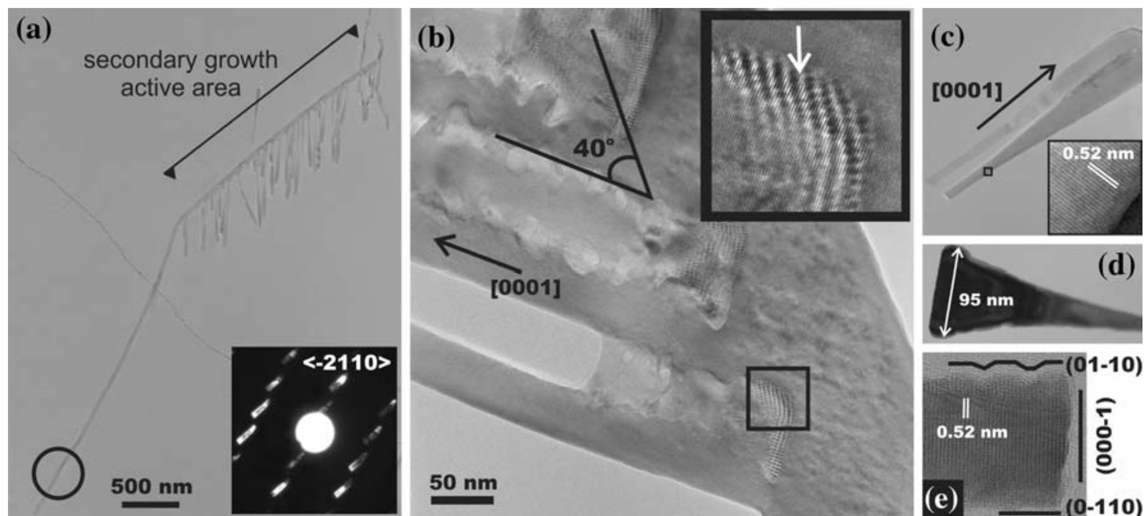

Fig. 4 (**a**) Image of a representative ZnO array of sample B. The secondary structures in this image are shaped as a baseball bat. The inset shows the defocused DP of the region signalled highlighting the undefined growth direction of the basal nanowires. (**b**) Enlarged view of an interface region where the secondary structures branch out from the basal nanowire. A clear difference of surface contrast is seen. Inset: Moiré interference fringes where the arrow marks the presence of a dislocation. (**c**) Baseball–bat-shaped structures with [0001] growth direction; the lattice image inset shows the (0002) planes. (**d**) Bright field image of a secondary structure with nail shape. (**e**) Narrow end of the structure in (**d**); one of the side surfaces is highly irregular

the half-plane points such as the one marked by the white arrow, reveals the presence of dislocations in the arrays. Additional diffraction contrast analysis carried out on isolated secondary structures, and using g = 0002 and g = −2110, concurred the absence of dislocations for these. This disparity in defect density between the basal nanowires and the secondary structures is also illustrated by the strong surface contrast variations observed (Fig. 4b). Accordingly, whereas the first show a spotty appearance, this most probably due to the presence of high surface roughness and defects clusters, the latter are seen to have regular surfaces.

As regards the chemical composition of the products of sample B, EDX analysis was carried out widely on the sample and no other elements were found besides Zn and O. Overall, this sample had thinner structures than sample A. The basal nanowires were grown in non-unique directions and branched into secondary structures of non-uniform shape but with regular orientation. Generally, the products of sample B, besides being less homogenous, contained more defects when compared to sample A.

I–V measurements

Sample A

The first set of *I–V* measurements for sample A was made using a ZnO array similar to those previously described (Fig. 2a). Before establishing the contact, an *I–V* curve was swept and, apart from a baseline offset of ca. −5 nA, the spectrum did not show any measurable signal (Fig. 5b, spectrum No contact). It is assumed that the offset is a consequence of charging of the holder electrodes due to their bombardment with high-energy electrons. In fact, it was seen that in the absence of the electron beam, the offset always disappeared. Although not many arrays were properly aligned, and the contact of these to both electrodes was highly challenging, it was still possible to acquire several spectra. A typical example is the structure in Fig. 5a which was tightly connected on both ends to the Au electrodes (tip and sample wire). An Ohmic-type linear relation was obtained from where it was possible to directly extract the resistance using the known expression, $R = dV/dI$ (see Array, Table 1). When the electron beam was blanked, the *I–V* curve rapidly decayed and no measurable signal was identified.

Following the analysis of the array, the electrical properties of a series of nail-shaped structures, which were highly asymmetrical and grew along [0001], were probed. The first example corresponds to a simple head-end measurement (Nail Contact 1, see Fig. 6a). The *I–V* curves showed a typical Schottky-type behaviour. Interestingly, these remained unaltered even after biasing the source electrode with −4 V. As can be observed from Fig. 6b, a linear relation can be assumed for the *I–V* plot in the large bias regime, i.e. $|V| > 5$ V. In accordance to a model recently proposed to explain the electrical characteristics of semiconductor nanowires [21], it was then possible to calculate the resistance of this structure resorting to this large bias region (Nail Contact 1, Table 1).

This experiment was followed by a more complicated design involving two free-standing nail-shaped structures

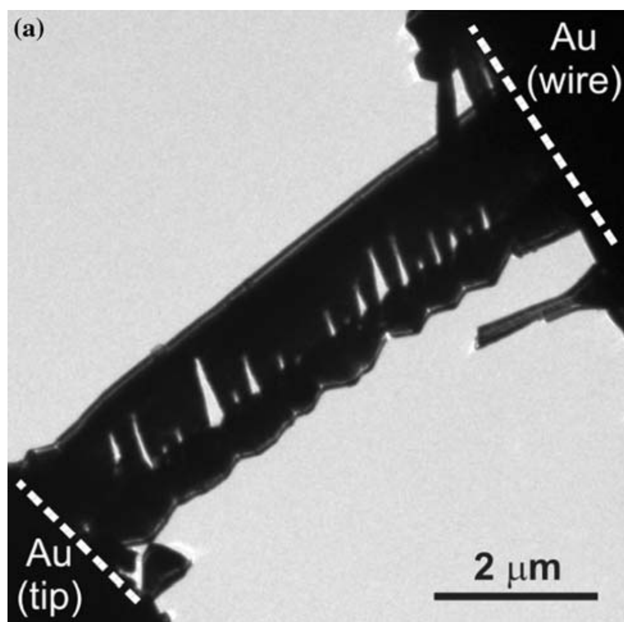

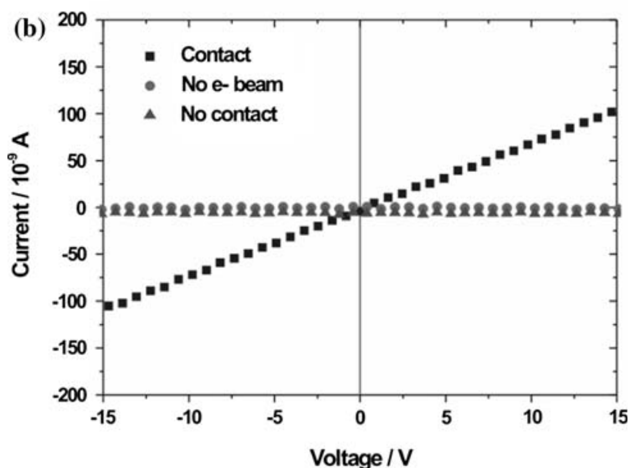

Fig. 5 (**a**) Cross-sectional view of a contacted array (sample A). (**b**) *I–V* curves of (**a**) taken in contact and non-contact modes. An additional measure was taken for a contact with no electron beam

Table 1 Calculated resistance values for sample A

Sample A	Array	Nail Contact 1	Nail Contact 2
Average resistance (MΩ)	185	413	263
Standard deviation (MΩ)	45	83	103

(Nail Contact 2, Fig. 6c). The contact established between the two nail heads was surprisingly stable throughout the *I–V* measurements. The initial curves showed pronounced Schottky-behaviour (Fig. 6d), in agreement to the previous example. However, after a few forward–reverse sweeping cycles, the current values changed and the characteristics went from being almost symmetrical to a more rectifying profile. No changes in the head–head contact were seen but it is possible that one of the nail–electrode contacts may have moved, thereby changing the electrical properties of the system. Analysis of the large bias regions gave an average resistance value of 263 MΩ (Nail Contact 2, Table 1).

In the next layout, this variable behaviour (i.e. alternating from almost symmetrical to almost rectifying) was confirmed. However, this time the head–head contact was not as stable. In fact, by slightly translating the sample wire electrode it was possible to change the position of the ZnO heads. Figure 7a–c shows a set of images (with respective spectra below) where the effect of varying the head contact can be followed. In the first of these, i.e. Fig. 7a, no contact has been established with the Au electrode (despite the appearance, the plane of projection of the nail is not the same as that of the electrode). When the contact was made, a symmetrical Schottky-type curve was obtained (Fig. 7b, e). Further contact modifications resulted in commensurate variations in the *I–V* curve, sometimes leading to behaviours close to rectifying (Fig. 7c, f).

Sample B

Due to the flexibility, heterogeneity of morphologies and higher density of defects in sample B structures, a more balanced distribution of behaviours (linear, symmetrical and rectifying) was anticipated. Surprisingly, the majority of the *I–V* curves followed Schottky-type patterns as shown in the inset of Fig. 8a. Furthermore, no Ohmic-type curves were obtained for this sample and (almost)-rectifying behaviours were seldom measured. A baseline offset was present although its absolute value was smaller than for sample A. Likewise, it would disappear the moment the electron beam was blanked. Additional experiments were performed in order to find whether the *I–V* curve would change with induced stress in the system. The set of images in Fig. 8a–c illustrates part of a deformation cycle that the structures were repeatedly submitted to. As can be observed from the inset plots, the elastic deformation of the array did not result in measurable changes in the *I–V* curve either in shape or absolute current values.

Using the intermediate bias regime (5–10 V) it was possible to numerically calculate a series of parameters other than resistance (Table 2). As pointed out in [21], in this bias regime, the reverse-biased Schottky barrier dominates the total current I,

$$\ln I = \ln(SJ) = \ln S + V\left(\frac{q}{kT} - \frac{1}{E_0}\right) + \ln J_s$$

where J is the current density through the Schottky barrier, S is the contact area associated with this barrier, E_0 is a

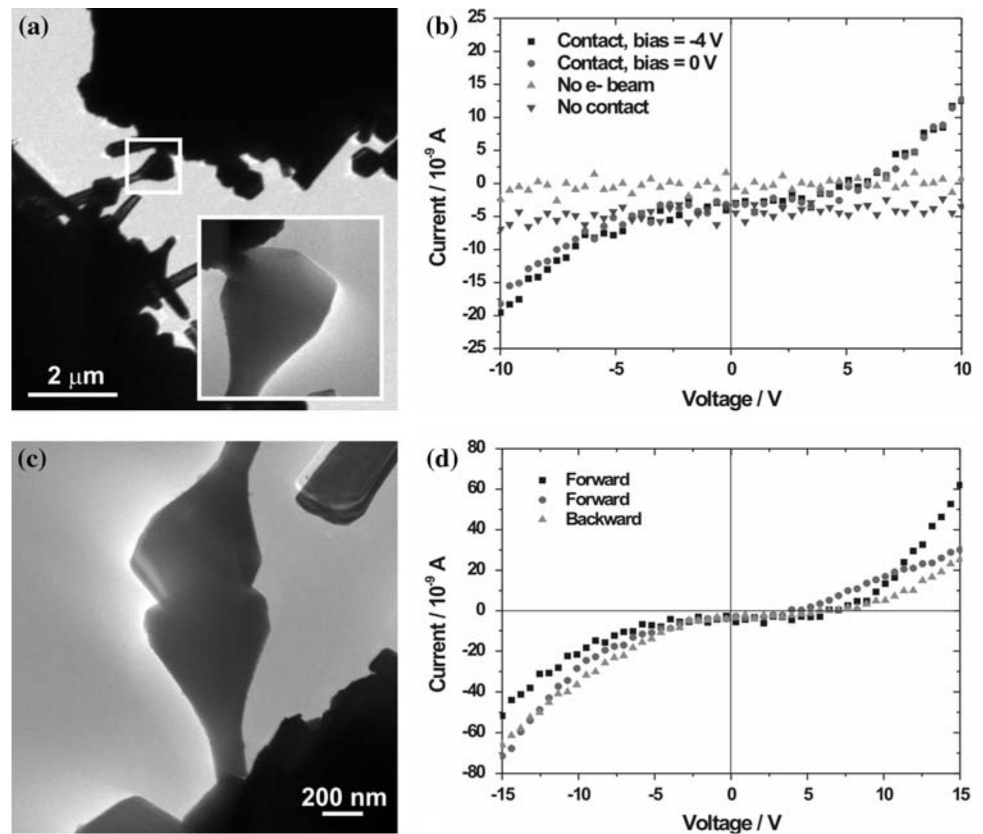

Fig. 6 (**a**) Nail Contact 1: contact of a nail-shaped secondary structure of sample A. Inset: detail of the head–electrode junction. (**b**) *I–V* curves of (**a**); besides the effect of the electron beam, the influence of an applied bias was studied. (**c**) Nail Contact 2: head–head contact of two nail shaped structures. (**d**) *I–V* curves of (**c**); the consecutive curves show a variation of the *I–V* characteristics

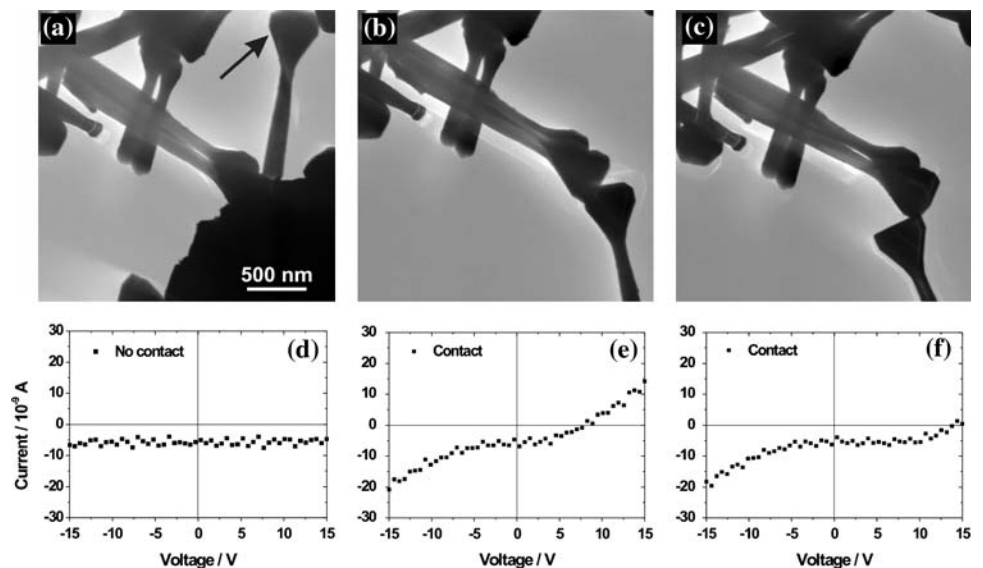

Fig. 7 (**a–c**) Sequence of images showing the establishment of a head–head contact and the possibility of changing it. The arrow in (**a**) marks the nail structure that was used to connect in (**b**) and (**c**). Despite appearance, no contact is present in (**a**). (**d–f**) Respective *I–V* curves of the images above them showing the evolution of the *I–V* curve with contacts variations (from almost symmetrical in (**e**) to almost rectifying in (**f**))

parameter that depends on the carriers density, and J_s is a slowly varying function of applied bias.

An interesting observation for this array was that the absence of the electron beam did not result in the immediate annihilation of the *I–V* signal. In fact, even for spectra taken some 5 s after beam blanking a clear *I–V* signal could still be read.

Following the electrical characterisation experiments, the array was subjected to increasing applied voltages between the two end-contacts. The purpose of this test was twofold: (a) to analyse its structural resistance and (b) to verify whether failure would take place at the high dislocation density interfaces between the primary and secondary structures. Video recording was carried out for a

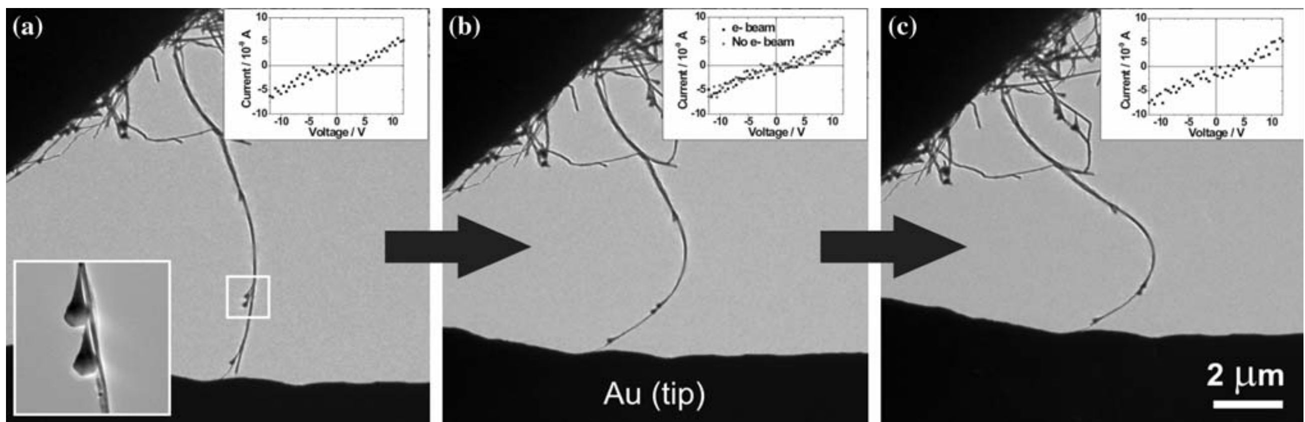

Fig. 8 Deformation cycles. (**a**) Starting position for an array of sample B. Inset: magnified image of secondary structures (bottom left corner) and a representative *I–V* curve (upper right corner). (**b**) Bending of the array does not change significantly the *I–V* curve in shape or current values. Furthermore, the effect of the electron beam is not noticeable. (**c**) Final stage of deformation. The significant bend demonstrates how flexible this array is. The *I–V* did not suffer any alterations

Table 2 Calculated electrical properties for sample B

Sample B	Array
Length (μm)	14
Diameter (nm)	95
E_0 (meV)	27.2
Electron concentration (/cm^3)	7.9E17
Resistance (MΩ)	1360
Mobility (cm^2/Vs)	0.90

period of around 2 min (available as Supplementary Material and [22]), and clearly demonstrates the failure of the array as the applied bias voltage is decreased from −10 V to −130 V. Initially, the contact of the array starts as a single connection of the primary nanowire to the tip. At 21 s, which corresponds to a voltage applied across the array of approximately −20 V, this changes to a configuration where the nearest secondary structure is also contacted. With further biasing, the array appears to become wider. This is not a result of sample rotation but instead of charging of the array. Charging has a notorious effect on the trajectories of the imaging electrons, severely altering the final object image obtained. Further into the experiment, it is visible that the array becomes progressively thinner in the interface regions of the two non-contacted nail-shaped structures present. Consequently, at 1 min and 58 s of recording time, corresponding to a bias voltage of −110 V, a fatal structural failure was observed.

Discussion

The ZnO structures used in this study were a degree of complexity higher than nanowires, the electrical properties of which have already been reported [10, 21]. It was our intention to identify whether factors such as the electron beam, different structural geometries and defect densities would have a significant effect on the *I–V* curves measured with the in situ piezo-holder.

Effect of the electron beam

As demonstrated in the characterisation section, the ZnO samples were composed of complex arrays. Structural defects, such as dislocations, were particularly abundant where the primary nanowires branched out to give secondary structures with variable geometries. Experiments into the damage sensitivity of materials to electron irradiation are necessary in order to understand how local structure and chemical composition may be altered by the imaging beam. One method to measure the electron dose received by the specimen, i.e. the current incident on the specimen per unit area for a given time, is to use a Faraday cage. In our experiments, with parallel electron beam, the current densities were calculated to be below 0.5 A cm^{-2}. Using the calculated current density (j) upper limit together with the well-know relation, $j = eNv$, where e represents the charge of the electron, N the number of electrons and v their velocity, it was possible to calculate quantitatively the maximum flux of particles (Nv), that is, the number of electrons traversing unit area per unit time. This gave a maximum flux density of electrons of 3E18 electrons/cm^2 s. Studies of irradiation damages mechanisms for ZnO materials have, in the past, been carried out at 1E19 electrons/cm^2 s flux densities [23]. The electron beam dose used in this work can not account for the defects presence and is considered to be below the threshold flux needed to appreciably affect the structure. The dislocations and other defects are therefore assumed as inherent to the structure synthesised. It is important to point

this out because, under a fairly converged electron beam, the high energies of the imaging electrons are sufficient to displace oxygen from the ZnO lattice and result in the formation of metallic zinc [24]. This would naturally have a major impact on the electrical properties of the samples.

Besides the above, it is expected that the interaction of the high-energy electrons with a semiconductor material will induce the formation of electron–hole pairs (e^-/h^+). In order to form one electron–hole pair, an energy, E_{eh}, of about three times the bandgap is required [25]. For ZnO this implies that $E_{eh} = 11.11$ eV (E_g (ZnO) = 3.37 eV). Consequently, for each 300 keV incident electron (E_o), approximately 30,000 electron–hole pairs will be created (E_o/E_{eh}). In view of these values, together with the electron flux density, it is possible to estimate the density of e^-/h^+ per unit time as 2.7E17 $(e^-/h^+)\cdot cm^{-2}\ s^{-1}$. Despite the enormous amount of e^-/h^+ pairs generated these are not likely to have a dominating effect on the current. In fact, previous studies on ZnO nanowires using in situ STM/TEM holders concluded that the current signal (tens of nA are typical values) was dominated by carrier injection (tunnelling) from the electrodes to the nanowires [9]. This phenomenon is stimulated by the incident imaging electrons which drive the excitation of the metal electrode (Au) electrons to higher energy states, enhancing tunnelling across the metal–semiconductor (M–S) Schottky barrier.

As regards sample A, the absence of a current signal when the beam is off may be due to the lower carrier density available in the structures. In fact, in the absence of the electron beam neither the injection current (tunnelling) nor the beam-induced current (e^-/h^+ pairs) are possible. It is, therefore, surprising that sample B still showed a clear signal when the electron beam was off. Spectra with no electron beam were taken, sometimes in sequences of 3, 4 consecutive spectra, at intervals of approximately 2 s each. The time span for the spectra acquisition is considerably larger than any processes of current decay or carriers recombination which means that the current signal can not be interpreted as part of a decay process. In fact, the free-exciton emission lifetime for ZnO is in the order of several hundreds of picoseconds [26]. Repeated verifications were made to ensure that no other contacts were present. We can not at this stage explain the reason for this discrepancy between the two samples.

I–V characteristics and resistance values

It is assumed that both Fermi surface alignment and the nature of the interfaces between the Au electrodes and the ZnO structures differ for the several examples analysed. Consequently, in the full set of spectra of samples A and B all types of expected *I–V* curves were observed. A model to explain these different characteristics for semiconductor nanowires, and based on the thermal field emission theory, was recently suggested [21]. However, due to the complexity of our structures other factors may also come into play.

Schottky barriers are formed at M–S interfaces (such as the Au/ZnO employed here). These barriers play a crucial role in the electrical transport of metal–semiconductor–metal (M–S–M) systems such as those commonly used for field effect transistors (FET). However, if the semiconductor is heavily doped, both M–S contacts may be reduced to Ohmic contacts resulting in linear *I–V* characteristics. This behaviour was observed for the array in sample A and provides circumstantial evidence that these arrays are slightly doped with In. According to the growth mechanism proposed [12], In is expected to concentrate in both ends of the primary basal structure. In spite of the difficulty to get a clear view of the M–S contact surfaces (due to tilt limitations and the presence of several other structures in the surrounding areas), we believe that these were established through the primary basal structure end surfaces. This implies the use of the non-polar crystal planes $\{11\bar{2}0\}$ and $\{01\bar{1}0\}$ which eliminates any possible effects played by spontaneous polarisation charges. Put together, this would explain the observed characteristics for the array since In–n–ZnO contacts have previously been demonstrated to have Ohmic behaviour at room temperature [2].

The rectifying behaviour is predicted by the thermionic emission theory if one contact is Ohmic while the other one remains Schottky-type. In spite of the dominance of the almost-symmetrical curves and the ZnO–Au contact being usually Schottky-type, some of the present structures, particularly for sample A, showed rectifying *I–V* characteristics. If we consider the nails structures of sample A, the polar and ionic character of the ZnO $(000\bar{1})$ surface can limit the probability of forming rectifying contacts because of surfaces states that are occupied by free electrons which need not form ionic bonds with O atoms. Conversely, the likelihood of surface states for the polar ZnO (0001) face is small as free electrons are unusual for this Zn-terminated surface. The immediate consequence of this is M–S contacts with different characteristics for the (0001) and $(000\bar{1})$ faces [18]. Unfortunately, we exerted no great control over the extension of the M–S contact surface since these nails were rigid structures and, unlike nanobelts, cannot be bent to increase the contact surface with the electrodes. We expect nonetheless that the nails–electrodes contacts are made through or very close to the ZnO {0001}-type planes. The extent to which the planes are aligned to the electrodes surfaces will control the type of behaviour observed (Fermi surface alignment). This was illustrated in our experiments, where the contact areas are seen to be of extreme importance. By controllably changing these (Nail Contact 2), it is possible to follow the

evolution of an almost-symmetrical to a more rectifying behaviour.

Conversely to the results recently reported by Wang et al. [10], where piezoelectric field changes are subsequent to deformations of ZnO nanowires, we could not identify significant effects on the *I–V* characteristics of our samples following their mechanical deformation. The higher amount of defects and more complex layout of the sample B array probed here, added to its lack of defined growth direction, could be factors that account for the contrasting results obtained.

Following the model developed for semiconductor nanowires [21], the resistance values were generally taken from the larger bias regions which follow linear *I–V* relations. It is interesting to note that our figures are much higher and variable than for any other ZnO nanostructures reported [10, 11, 21], which usually fall within the interval 80–120 MΩ. Notably, resistances for sample A were consistently lower than those for sample B. Dislocations and other type of lattice defects, such as vacancies, can act as current scatterers or recombination centres (carrier traps), ultimately increasing the resistance of the material to current flow. Overall, the present results indicate that the lack of a precise and constant growth direction in tandem with a considerable amount of defects will lead to high resistance values in nanostructures.

Structural failure

It is known that increasing an applied voltage will result in the proportional elevation of the local temperature of conductors through a phenomenon called Joule heating. The injected thermal energy is a consequence of the momentum transfer which occurs from the collision of charge carriers with lattice atoms. During our resistive heating experiments it is expected that, when increased values of bias were applied, temperature gradients along the nanostructures were established. In addition, high-resistance points, or 'hot spots', occurred at the interface region between the primary and secondary structures where previously a high concentration of defects had been identified. This effect, together with the concurrent high current densities, enhanced considerably electromigration. As a result, the ionic diffusion process progressively drove the array of sample B to failure, which took place precisely at the closest non-contacted high-resistance points to the tip-electrode.

Conclusions

In this work, it was shown that the electrical properties of ZnO low-dimensional structures can be successfully investigated using an in situ STM/TEM holder. These structures represent a higher degree of complexity from previous reports in the literature using this type of instrumentation. The high density of defects present in the ZnO arrays accounts for the elevated resistances measured. Moreover, this property is also seen to be related to the growth direction of the structures. Finally, it was demonstrated that areas with high density of dislocations will act as structural failure points. On the whole, and as concerns the electrical properties of nanostructures, it is concluded that the presence of defects is a dominating factor in the electrical properties of these nanostructured materials. This further illustrates the importance of a complete diffraction contrast analysis previous to any properties measurements, a fact that has sometimes been overlooked in the nanoscaled materials literature.

Acknowledgements We are grateful to Dr Yoichiro Uemura and Mr Keiji Kurashima for technical assistance. Dr Ujjal K. Gautam is thanked for useful discussions. Dr Oleg Lourie, from Nanofactory Instruments AB, is acknowledged for his continuous support. We are indebted to Prof. J. M. Zuo for the use of WebEMAPS (http://emaps.mrl.uiuc.edu/).

References

1. Vigue F, Vennegues P, Vezian S, Laugt M, Faurie J-P (2001) Appl Phys Lett 79:194
2. Jiao SJ, Zhang ZZ, Lu YM, Shen DZ, Yao B, Zhang JY, Li BH, Zhao DX, Fan XW, Tang ZK (2006) Appl Phys Lett 88:031911
3. Ding Y, Wang ZL (2004) J Phys Chem B 108:12280
4. Huang MH, Mao S, Feick H, Yan H, Wu Y, Kind H, Weber E, Russo R, Yang P (2001) Science 292:1897
5. Svensson K, Jompol Y, Olin H, Olsson E (2003) Rev Sci Instrum 74:4945
6. Svensson K, Olin H, Olsson E (2004) Phys Rev Lett 93:145901
7. Minor AM, Asif SAS, Shan Z, Stach EA, Cyrankowski E, Wyrobek TJ, Warren OL (2006) Nat Mater 5:697
8. Huang JY, Chen S, Wang ZQ, Kempa K, Wang YM, Jo SH, Chen G, Dresselhaus MS, Ren ZF (2006) Nature 439:281
9. Jin CH, Zhang ZY, Wang JY, Chen Q, Peng L-M (2006) Appl Phys Lett 89:213108
10. Wang XD, Zhou J, Song JH, Liu J, Xu N, Wang ZL (2006) Nano Letters 6:2768
11. Arnold MS, Avouris P, Pan ZW, Wang ZL (2003) J Phys Chem B 107:659
12. Shen G, Bando Y, Chen D, Liu B, Zhi C, Golberg D (2006) J Phys Chem B 110:3973
13. Shen G, Bando Y, Lee C-J (2005) J Phys Chem B 109:10578
14. Golberg D, Mitome M, Kurashima K, Zhi CY, Tang CC, Bando Y, Lourie O (2006) Appl Phys Lett 88:123101
15. Bando Y, Mitome M, Golberg D, Kitami Y, Kurashima K, Kaneyama T, Okura Y, Naruse M (2001) J Jpn Appl Phys 40:L1193
16. "Nanofactory Instruments AB", http://www.nanofactory.com/, as on 9/8/2007
17. Bonasewicz P, Hirschwald W, Neumann G (1987) Appl Surf Sci 28:135
18. Coppa BJ, Fulton CC, Kiesel SM, Davis RF, Pandarinath C, Burnette JE, Nemanich RJ, Smith DJ (2005) J Appl Phys 97:103517

19. Wang ZL, Kong XY, Zuo JM (2003) Phys Rev Lett 91:185502
20. Reimer L (1989) Transmission electron microscopy. Springer, Berlin
21. Zhang ZY, Jin CH, Liang XL, Chen Q, Peng L-M (2006) Appl Phys Lett 88:073102
22. "NIMS Nanotubes Group", http://www.nims.go.jp/nanotube/JMatScience2007.html, as on 15 August 2007
23. Yoshiie T, Iwanaga H, Shibata N, Ichihara M, Takeuchi S (1979) Philos Mag 40:297
24. Devenish R, Bullough T, Turner P, Humphreys C (1990) Inst Phys Conf Ser 98:215
25. Amelinckx S, Dyck DV, Landuyt JV, Tendeloo GV (1997) Electron microscopy – principles and fundamentals. VCH, Weinheim
26. Wilkinson J, Ucer KB, Williams RT (2004) Radiat Measure 38:501